JOURNAL OF AIRCRAFT
Vol. 45, No. 3, May–June 2008

Improving Aircraft Endurance Through Turbulent Separation Control by Pulsed Blowing

Domenico P. Coiro,* Ernani F. Bellobuono,† and Fabrizio Nicolosi‡
University of Naples Federico II, 80125 Naples, Italy
and
Raffaele Donelli§
Italian Center for Aerospace Research, 81043 Capua, Italy

DOI: 10.2514/1.33268

Boundary-layer unsteady blowing is one of the most advanced solutions for reducing aircraft parasite drags and flow separation at high angles of attack. It allows high lift along with low drag to be achieved and, because endurance is one of the most important performance parameters for certain types of aircraft, such as unmanned aerial vehicles, clearly the $CL^{3/2}/CD$ ratio has to be maximized. The main goal of the present investigation is to explore possible ways to obtain efficient turbulent boundary-layer control and, at the same time, to consider the practical problems connected to the installation of the device in a real wing. This study seeks mainly to verify the effectiveness of active control via pulsed blowing as a tool to delay boundary-layer separation. Numerical simulations and wind-tunnel experimental investigations on a wing model equipped with instruments are presented and the results discussed. An extensive numerical and experimental investigation on the parameters that can affect flow separation has been carried out. As a result of this analysis, it seems that tubing length produces the most significant effect on the resonant frequencies of a pulsed-blowing system, whereas slot exit and cavity volume mainly affect the resonant peak amplitude. The best actuation frequency varies, depending on the type of aerodynamic performance to be optimized (efficiency, lift, or endurance).

Nomenclature

C_f	=	skin friction coefficient
CL, CD	=	3-D lift and drag coefficients
Cl, Cd	=	2-D lift and drag coefficients
Cp	=	pressure coefficient $(p - p_\infty)/(0.5\rho U_\infty^2)$
$C_{t,c}$	=	acoustic compliance (with subscript t for tube and c for chamber)
C_μ	=	total momentum coefficient of pulsed-blowing jet
c	=	airfoil chord
c*	=	speed of sound
$\langle c_\mu \rangle$	=	mean part of momentum coefficient of pulsed-blowing jet
$c_{\mu\text{rms}}$	=	root mean square of momentum coefficient
$c'\mu$	=	fluctuating part of momentum coefficient of pulsed-blowing jet
d	=	diameter of connection tube in the pulsed-blowing system
E	=	efficiency
end, endurance	=	endurance parameter $CL^{3/2}/CD$
F^+	=	reduced frequency $(f^* X_{\text{act}}/U_\infty)$
f	=	frequency of pulsed-blowing jet
G	=	conductance (with subscript t for tube and c for chamber)
h	=	slot height
k	=	turbulent kinetic energy
L	=	acoustic inertance (with subscript t for tube and c for chamber)
Lt	=	length of connection tube in the pulsed-blowing system
p, p', p_∞	=	mean, fluctuating, and freestream pressure
q, q'	=	mean and fluctuating flow rate
R	=	resistance (with subscript t for tube and c for chamber)
Re_∞	=	freestream Reynolds number
St	=	Strouhal number
St_ν	=	viscous Stokes number
t	=	time
t^+	=	nondimensional time
U	=	total velocity of pulsed-blowing jet
U_{mean}, U'	=	mean and fluctuating velocity of pulsed-blowing jet
U_{rms}	=	root mean square velocity of pulsed-blowing jet
U_∞	=	freestream velocity
v	=	volume of actuator chamber
X_{act}	=	distance between slot cut and trailing edge
x, y, z	=	Cartesian coordinates
Y	=	acoustic admittance (with subscript t for tube and c for chamber)
y^+	=	spatial coordinate in the law of the wall variables
Z	=	acoustic impedance

Greek

α	=	angle of attack
ε	=	turbulent dissipation rate
θ	=	angle of flow injection
ν	=	kinematic viscosity
ρ	=	density
ω	=	jet pulsation or specific dissipation rate

I. Introduction

IN RECENT years, active flow control has once again become a research area in the aerospace community. Active flow control

Presented as Paper 4428 at the 25th AIAA Applied Aerodynamics Conference, Miami, Florida, 25–28 June 2007; received 4 July 2007; accepted for publication 25 November 2007.

*Professor, Department of Aerospace Engineering, Via Claudio 21.
†Ph.D., Department of Aerospace Engineering, Via Claudio 21.
‡Senior Researcher, Department of Aerospace Engineering, Via Claudio 21.
§Researcher, Via Maiorise.

differs from passive flow control in that auxiliary power is required. Such techniques can be applied to improve the performance of many aircraft, according to the result desired. For example, delaying separation enhances aerodynamic performance and improves landing characteristics as well as reducing acoustic noise. Furthermore, reducing or eliminating the moving surfaces required could lead to a more simple and efficient airframe. The endurance of high altitude and long endurance (HALE) unmanned air vehicles (UAVs) can also be greatly increased because the aircraft can fly with a high lift coefficient when cruising with low drag, thus achieving a high $CL^{3/2}/CD$ ratio. The suction side of this type of wing is dominated by separation areas that comprise large and small vortices with a wide range of lengths and frequencies. Recent experimental and numerical evidence has shown that, at high angles of attack, it is indeed possible to increase lift by controlling the vortex responsible for the process of separated flows. Many researchers have studied the effectiveness of such techniques (Eppler [1] for suction, Seifert and Wygnanski [2], Seifert et al. [3], Tinapp and Nitsche [4], Kim and Williams [5], Gad-el-Hak [6], and Wu et al. [7] for unsteady blowing and synthetic jet). The current challenge is twofold: on the one hand to improve the application on real flying wings and, on the other, to acquire a better understanding of the physical behavior.

The goal of this research project is to investigate both the effectiveness of unsteady-blowing techniques as tools for turbulent separation control and the technology solutions to practically implement the unsteady-blowing device in a real wing. We show that such a technique, which has already been proven to be applicable to multicomponent airfoils, in particular for flaps with large separation areas, can also be applied to a HALE wing surface in a cruise configuration. Typically, cruising conditions mean a low angle of attack, but this airfoil has been designed for the following requirements: high altitude (more than 20 km) and long endurance. Under these low Reynolds flow conditions, engine efficiency has to be maximized to satisfy the long endurance requirement. As a consequence, the airborne vehicle needs to fly with a high lift coefficient and minimum engine power. This means a high angle of attack and a possible separation in cruising conditions.

The investigations performed were both numerical and experimental. The numerical simulation of a pulsed-blowing system was done to highlight how aerodynamic performance depends on geometrical parameters to drive the design of the experimental test. The numerical results were used to design mechanical interchangeable parts suitable to investigate the most critical parameters experimentally. The paper starts with numerical simulations of unsteady blowing. The numerical investigation of the effectiveness of unsteady blowing on a 2-D single component airfoil was performed using the Reynolds-averaged Navier–Stokes (RANS) approach (with FLUENT), with the goals being to investigate the best range of actuation frequencies, injection angles, and blowing mass flow rate by evaluating lift improvement and drag reduction.

This section continues with some preliminary considerations about pulsed-blowing systems and the design and building of an ad hoc rotating valve to produce excitation correctly. A theoretical model of a pulsed-blowing system is studied using an electroacoustic analogy, which highlights the interdependence of resonance with geometrical parameters.

In the experimental part, two tests were performed (see Fig. 1): the first on a small scale model (21 cm in span and 40 cm in chord) and the second on a full span model (1.4 m). The small scale model was used firstly to carry out preliminary tests on the effectiveness of steady suction and to characterize the pulsed-blowing system (rotating valve-tube actuator) and, secondly, to gain experience and understanding of the main technological problems. In fact, the small scale model experimental setup has pointed out some problems, such as the connection between the tube and chambers and slot cut building techniques, in particular the wrong orientation and position of the cut in the closing plate and the shape of chambers. These problems were solved during the design and building of the full span model (1.4-m span and 0.6 m in chord). In this paper, the design and building of the full scale model is presented with the system setup in the wind tunnel. Initially, the tests are presented on a baseline configuration without control activated for both the free and fixed transitions. Subsequently, we present the results with the application of control (steady and unsteady blowing) and report on the effects of the angle of attack, frequencies, and Reynolds number. In Fig. 1, vortex generators are also present as possible devices in addition or as alternatives to unsteady blowing, but they will not be considered in this paper.

II. Two-Dimensional Numerical Simulation

A. Settings and Grid

A numerical investigation of active flow control by steady and unsteady blowing is presented, as this can make significant aerodynamic improvements to aircraft performance by suppressing or limiting the detrimental effects of separated flow.

Many experimental studies (Seifert and Wygnanski [2], Tinapp and Nitsche [4], Wu et al. [7,8], and Miranda [9]) and numerical investigations (Schatz and Thiele [10], Ekaterinaris [11], and Liu and Sankar [12]) have looked at the effectiveness of active flow control as a tool to delay boundary-layer separation paying particular attention to leading-edge separation on the flap in multicomponent airfoils. For the majority of applications, this technique is mainly applied to enhance aircraft performance during takeoff and landing. Our aim

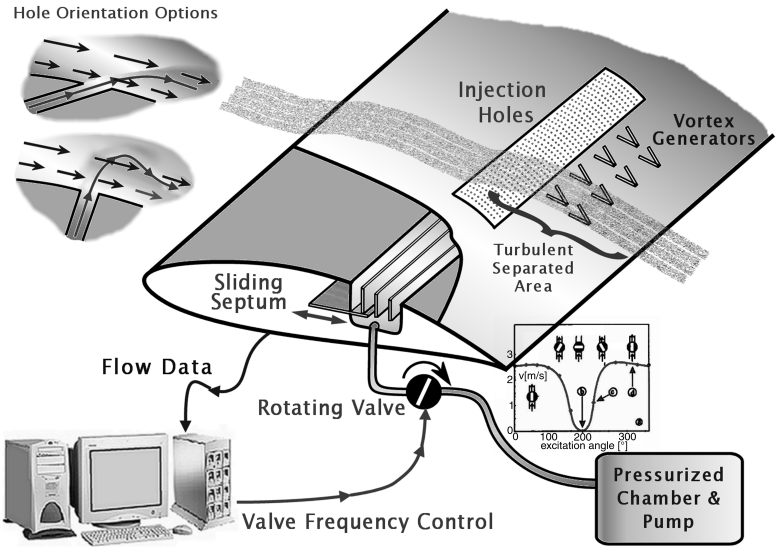

Fig. 1 Scheme of experimental setup.

was to verify numerically the effectiveness of this technique to delay or suppress separation on a single component airfoil in the prestall area, focusing on cruising conditions. As mentioned in the Introduction, the endurance of HALE UAVs is a performance parameter that would also benefit from applying flow control.

The experimental work of Seifert and Wygnanski [2], Seifert et al. [3], and Tinapp and Nitsche [4] showed the effectiveness of active control to be highly dependent on actuation frequency and strength. Oscillatory blowing is about 1 order of magnitude more efficient than steady blowing, especially if the process is actuated by frequencies that correspond to the most unstable frequency of free shear layer detaching from separation point. The coefficients of reduced frequency and momentum are indicated in Eqs. (1) and (3), X_{act} is the distance between the actuation and trailing edge, h is the slot height, and f is the frequency of disturbance to the flowfield. The reduced frequency is also known as a "scaled" Strouhal number [Eq. (2)], for which the characteristic length used is X_{act}. An alternative definition of the momentum coefficient is indicated in Eq. (4) using the root mean square of the velocity (mainly used for the experimental characterization).

$$F^+ = \frac{f^* X_{\text{act}}}{U_\infty} \tag{1}$$

$$St = \frac{f^* c}{U_\infty} \tag{2}$$

$$C_\mu = \langle c_\mu \rangle + c'_\mu = \frac{2h}{X_{\text{act}}}\left(\frac{U_{\text{mean}}}{U_\infty}\right)^2 + \frac{2h}{X_{\text{act}}}\left(\frac{U'}{U_\infty}\right)^2 \tag{3}$$

$$C_{\mu\text{rms}} = \frac{2h}{X_{\text{act}}}\left(\frac{U_{\text{rms}}}{U_\infty}\right)^2 \tag{4}$$

The momentum coefficient comprises the mean and a fluctuating value. If the mean is higher than the fluctuating amount, then the flow injection is always more than zero, and a small amount of steady blowing is present (close to reality). If the mean and fluctuating amounts are equal, then the pulsating blowing is pure. This case is less realistic but it is the one that we have chosen to consider to better isolate the effect of unsteadiness compared with the steady effects.

Seifert and Wygnanski [2] stated that, although relatively large quantities of steady blowing ($c_\mu = 2$–10%) near the point of separation can delay separation or reattach the flow and increase lift, steady blowing may also cause a thickening of the boundary layer and the wake behind the airfoil, which could lead to increased drag and be detrimental to overall efficiency. In contrast, pulsed blowing takes advantage of inherent local instabilities in the near-wall shear layer that detaches from the surface and causes the selective amplification of the input oscillation frequency. Convective motion shifts these disturbances downstream along the surface as coherent large structures to promote mixing between the high and low momentum flow and contribute to the delay of separation. Pulsed blowing has proven to be a reliable technique for separation control with the most effective location for unsteady forcing near the point of separation, and with the optimum reduced frequency for oscillations of $F^+ \approx 1$.

A sensitivity analysis of frequency, momentum, and jet injection angle is presented. The numerical simulation is based on RANS equations with FLUENT version 6.1.22, developed and marketed by Fluent, Inc. The meshing software used was Gambit, which is available with FLUENT. The pulsating disturbance to the flowfield is imposed as indicated in Eq. (5), in which the fluctuating part as a sinusoidal wave form is superimposed on the mean value of injection U_{mean}. The maximum fluctuation is equal to the mean value, and the minimum velocity is zero. By changing frequency f, it is possible to do a sensitivity analysis using frequency, and steady blowing is obtained from the same formula by considering the frequency equal to zero. Momentum coefficient effects can be studied by changing the amount of mean velocity U_{mean}.

$$U(t) = U_{\text{mean}} + U' = U_{\text{mean}} + U_{\text{mean}} * \sin(2\pi f t) \tag{5}$$

The airfoil investigated was designed by Italian Center for Aerospace Research (CIRA) researchers (see Fig. 2). This airfoil was designed using the "Stratford" pressure recovery criteria, thus it is characterized by an upper surface pressure recovery designed to have a skin friction coefficient close to zero. To simulate a realistic "construction" situation, a slot cut slightly modifies the geometry of the airfoil locally, to create an inlet for pulsating flow. An estimation of the effects of the step was carried out. The aerodynamic performance of the wing configuration both with and without the step was computed. The results showed that the step did not significantly affect performance because it is located in the turbulent region of the wing.

The slot exit has a dimension of 0.8 mm and can be modeled as a wall boundary condition (no control applied) or as an inlet boundary condition (steady and unsteady blowing). It is possible to vary the inlet velocity orientation simply by modifying the angle between the velocity and the normal to the slot without modifying the geometry. The slot exit position was determined from preliminary numerical and wind-tunnel experiments performed on a small scale model. From these analyses, the separation location in the cruise condition was found to be around 70% in chord. Based on this, the injection point was located just upstream ($\approx$60%) of the flow separation.

The information acquired from these preliminary tests on a small scale model was used to optimize the design and testing of unsteady blowing on the full scale model. The computational C-type grid is illustrated in Fig. 3. It was designed with 2 blocks for a total of 31,500 cells, the first with 340 points on the airfoil (opportunely clustered to provide definition at the leading edge, slot, and trailing edge) and 60 normal to the wall and the second surrounding the first with a transition zone from 360 points to 120 and 35 points in the normal direction. Two additional grids with 22,000 and 75,000 cells were tested without substantial differences in the results. In the wake, 60 points were used and the grid was extended from 15 chords upstream of the leading edge to 20 chords downstream of the trailing edge. The number of points in a streamwise direction was kept high for the reason that this airfoil was designed using the Stratford skin friction distribution criteria and is therefore characterized by a strong upper surface pressure recovery and a skin friction close to zero for a substantial part of the upper surface.

To correctly capture this behavior, the maximum aspect ratio of the cells near the surface was kept below 100, and the first cell height was fixed at 3×10^{-5} m ($Y^+ \cong 1$).

Solver settings are implicit and segregated (the equation set is solved sequentially) with a second order in space and time. The pressure correction algorithm is a semi-implicit method for pressure-linked equations consistent (SIMPLEC). Boundary conditions are the velocity inlet far upstream of airfoil (with a velocity module of 18.7 m/s equivalent to Re_∞ of 8×10^5),the periodic on the top and bottom of the domain, and the pressure outlet far downstream. The profile surface is considered to be a no-slip wall except for the slot that can be considered both wall (when actuation is not activated) and velocity inlet (when actuation is activated), given the definition of user defined function. Inlet turbulence is kept low at an intensity of less than 0.1% (Department of Aerospace Engineering wind-tunnel turbulence level).

The aerodynamic performance of this type of airfoil (Stratford recovery) depends greatly on transition location; pressure distribution changes drastically when the position of transition moves slightly downstream or upstream. We were keen to avoid the effects

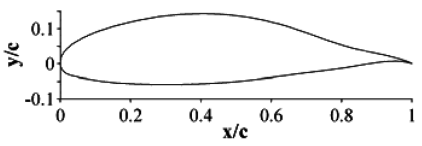

Fig. 2 Airfoil designed at CIRA.

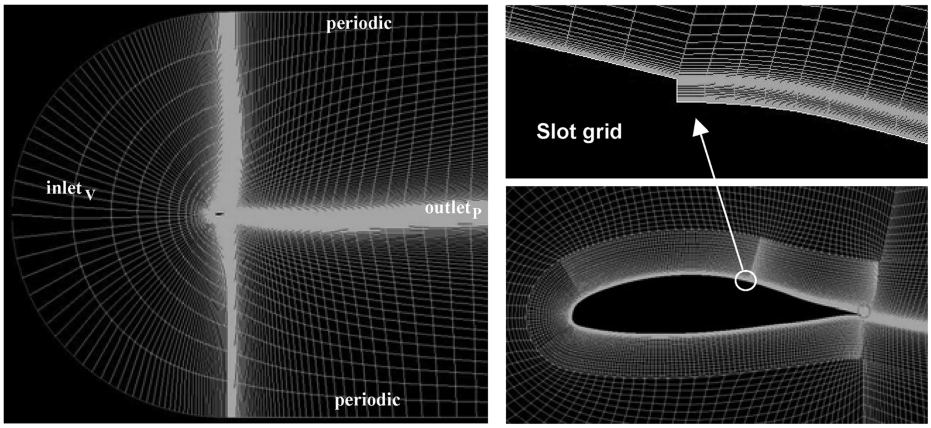

Fig. 3 Computational grid: a) boundary conditions, and b) close ups (airfoil and slot).

not directly dependent on control to isolate the effectiveness of blowing (by eliminating other effects) for its evaluation. The transition point was therefore set at 4% of chord on the upside and 50% on the lower side. In this configuration, the flow conditions are close to full turbulence. Many turbulence models are available in FLUENT. A variation of the standard k–ω model, called the k–ω shear stress transport (SST) model, was developed by Menter to effectively combine the robust and accurate formulation of the k–ω model in the near-wall region with the freestream independence of the k–ε model in the far field [13]. These characteristics make the k–ω SST model more accurate and reliable over a wider range of flows, particularly for airfoil flows, compared with the standard k–ε model. The k–ω SST model was used for the computations presented herein.

For unsteady calculations, an appropriate time stepping should be used. For situations in which no control is applied, and even though the simulation can be done in steady conditions, at a high angle of attack high separation occurs, and the flow becomes intrinsically unsteady. For this reason, even when control is "off," the unsteady simulation is performed and a nondimensional time stepping equal to 0.01 is used as indicated in Eq. (6), c is the airfoil chord. This is equivalent to choosing a sampling rate of 3 kHz (more than enough to capture unsteadiness for frequencies of up to 100 Hz).

$$\Delta t_1^+ = \frac{\Delta t^* U_\infty}{c} \tag{6}$$

B. Results: Frequency Effect

In this section, the control is activated with steady and unsteady blowing at different frequencies, and the results are compared with the baseline data obtained in the previous section. First of all, the frequency effect is analyzed by varying only the pulsation of the injected flow, with the momentum coefficient kept constant. In the second part, the effect of the momentum coefficient is presented by varying the mean velocity and keeping the frequency constant. The law of control has the wave form indicated in Eq. (5) with mean velocity of 15 m/s. This velocity corresponds to the momentum coefficient $C_\mu = 4 \times 10^{-3}$ (0.4% of added momentum compared with the freestream momentum).

Five different actuation frequencies were numerically tested, 0, 30, 50, 80, and 120 Hz (F^+ from 0 to 1.5), over angles of attack ranging from 4 to 25_deg. A value of 0 Hz means that only the steady part is activated (steady blowing). The aim is to identify at each angle of attack the frequencies (either one or more than one) that best "lock" with the flow structure and eventually formulate a general rule to predict system behavior. It is also important to monitor both the lift and drag; in fact, it is not assumed that an optimal condition for lift would coincide with the condition that also maximizes the drag reduction. The numerical simulation was carried out starting from the steady solution and applying sequentially first steady blowing and then pulsating control at $f = 30$, 50, 80, and 120 Hz (F^+ from 0.4 to 1.5). The time duration for each frequency is not preset, as transient time could vary when actuation frequencies are changed. One example of a complete simulation is reported in Fig. 4 for a 9_deg angle of attack. The lift (Fig. 4a) and drag (Fig. 4b) responses with frequencies are compared with the uncontrolled case and the steady blowing case.

In Fig. 5, the results with activated control are shown giving the percentage difference in lift and endurance with respect to the uncontrolled case. In Fig. 5, it is possible to see that the gain in lift (Fig. 5a) changes with the angle of attack and frequency differently from the gain in endurance (Fig. 5b). For example, considering the angle of attack of 12_deg, the best lift enhancement is obtained at a frequency of 30 Hz [$F^+ = 0.4$ (circle)] and is equal to 23%, but for endurance the best frequency becomes 50 Hz [$F^+ = 0.64$ (triangle)]. This nonuniform behavior is also found at 15 and 18_deg. Another point worth noting is that, even when focusing on a single

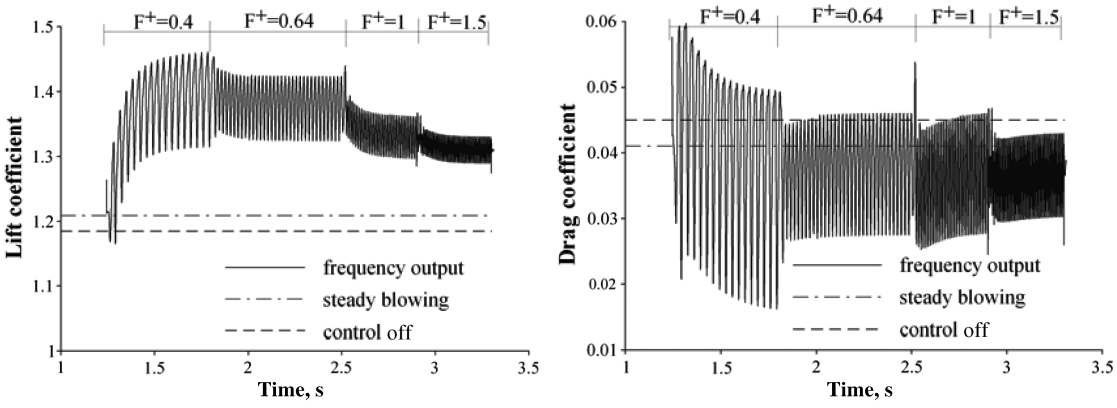

Fig. 4 Complete unsteady simulation at a 9_deg angle of attack compared with the uncontrolled case: a) lift coefficient, and b) drag coefficient

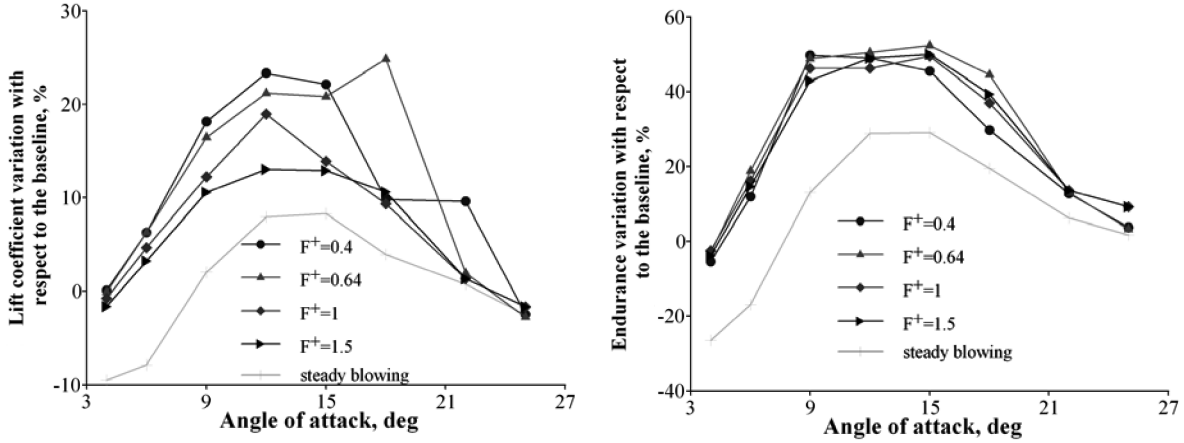

Fig. 5 Percentage variation with respect to the uncontrolled case: a) lift coefficient, and b) endurance.

characteristic, for example, on lift, there is no single optimal frequency for all angles of attack. The curves for lift shows that the frequency of 30 Hz ($F^+ = 0.4$) gives the best performance up to an angle of attack of 15_deg.

For an α of 18_deg, the curve relating to a frequency of 30 Hz ($F^+ = 0.4$) falls, and the increase in lift relating to pulsation at a frequency of 50 Hz ($F^+ = 0.64$) becomes greater. In brief, for lift at low angles of attack, the low rather than the high frequencies produce better results, whereas the opposite occurs at high angles. If endurance is the main target to be maximized, then drag also has to be considered, and the frequencies 50 and 80 Hz produce better results overall. The frequency of 30 Hz is the one that shows the best results at lower angles compared with the others, and it is the best at high angles, whereas the frequency of 50 Hz is the best if endurance is taken into consideration. These differences in the optimal frequency for lift are probably due to the fact that the most unstable frequency in the shear layer detaching from the airfoil surface changes at different angles of attack, and the actuation that best "locks" with it changes as a result. However, if the wake is also taken into account in the mechanism of interaction (and consequently the prime objective becomes endurance), then a more regular pattern of behavior can be detected, as shown in Fig. 5b in which the frequency of 50 Hz ($F^+ = 0.64$) seems to give the best results.

C. Results: Momentum Effects

The momentum coefficient defined in Eqs. (3) and (4) is studied in this section to see how aerodynamic performance changes by varying its intensity. The analysis was carried out by keeping the angle of attack and the actuation frequency fixed and varying only the mean velocity to modify the momentum coefficient. Four levels of mean velocity were tested (5, 10, 15, and 25 m/s), and the movements in lift and drag coefficients are illustrated in Figs. 6 and 7. The angle of attack was set at 12 deg and the actuation frequency at 50 Hz for all four momentum coefficients considered. It can be seen that actuation benefits lift even at a low intensity ($C\mu = 0.001$) and that lift tends to become greater as the momentum coefficient rises. It is important to point out that the marginal gains in endurance are lower than the increases in momentum. In fact, as reported in Table 1, if the momentum coefficient doubles from 0.004 to 0.008, then the endurance increases from 29 to 36 (+24%), and if the momentum increases fivefold from 0.004 to 0.02, then the endurance increases from 29 to 51 (+75%).

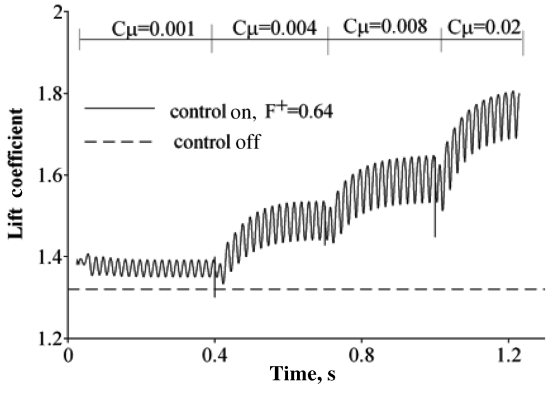

Fig. 6 Lift history with varying $C\mu$. Comparison between the frequency output at 50 Hz ($F^+ = 0.64$) and the uncontrolled case.

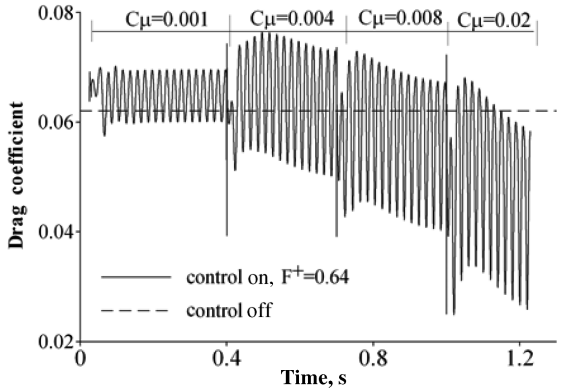

Fig. 7 Drag history with varying $C\mu$. Comparison between the frequency output at 50 Hz ($F^+ = 0.64$) and the uncontrolled case.

D. Results: Jet Angle Effects

In this section, the effect of the injection angle is analyzed. The injection angle is the angle between the velocity and the normal to the surface boundary of the slot, as illustrated in Fig. 8.

It is important to analyze this effect to understand whether or not a small amount of injection in the direction tangential to the surface body is useful in terms of lift enhancement or drag reduction. Even in the aforementioned case, the injection is not perfectly tangential to the surface as it is impossible to create tangential blowing without totally modifying the upper surface of the airfoil. What remains to be understood is whether this nonperfect alignment with flow could be beneficial or detrimental as this information would be useful for optimizing the design of the model for wind-tunnel testing.

Table 1 Summary of results for momentum effects

C_μ	U_{mean}, m/s	C_l	C_d	End
0.000	0	1.320	0.062	24.46
0.001	5	1.375	0.066	24.62
0.004	10	1.495	0.063	29.01
0.008	15	1.600	0.055	36.80
0.020	25	1.755	0.045	51.67

To examine the influence of the injection angle, the strategy adopted was to set the configuration (angle of attack = 12 deg) and, starting from this point, to test five different injection angles (from 0 to 40 deg) while keeping the momentum coefficient and reduced frequency fixed ($f = 30$ Hz). The results are reported in Fig. 9, in which endurance is illustrated for the five cases examined.

As can be seen in Fig. 9, an increase in the injection angle produces progressive decreases in endurance. Another important point is that the general rate of decrease is not steady, and the rate grows as the injection angle exceeds 10 deg.

This indicates that for both lift and drag the most favorable situations are when injection is tangential to the airfoil surface. The information acquired from this numerical analysis was used as general criteria to design and build an experimental model for testing in the Department of Aerospace Engineering (DIAS) wind tunnel. The criteria covered the following design aspects: the location of the slot exit for suction and blowing, the power required to operate suction, the optimal frequency for the rotating valve design, and the orientation of the slot exit for pulsed blowing.

III. Pulsed-Blowing System: Modeling and Simulation

Oscillatory actuators fall into two general categories, zero-net mass (synthetic jets) and pulsed blowing. Synthetic jets are self-contained with a zero-net-mass addition to the flow, whereas pulsed-blowing actuators require a source of pressurized fluid, resulting in a nonzero average flow across the actuator interface.

The unsteady-blowing scenario was investigated using a rotating valve-tube-actuator resonant system. The numerical evaluation of the influence of each element in the complete system chain was carried out very carefully to find the optimal values for the reduced frequency output velocity as well as for the unsteady and steady components of the momentum coefficient needed to improve aerodynamic performance. With regard to this, some previous experimental work [2,4] on different model setups indicated that the oscillatory flow component should promote mixing between the higher and lower momentum fluids, causing the reattachment of the flow. In practice, the pulsed-blowing system can be obtained through a steady air supply modulated by a rotating valve to produce unsteady excitation that is transmitted to the actuator (cavity) by a transmission line (tube). The input voltage for the rotating valve (round per minute) controls the rotation frequency, and a single valve can be designed to supply more than one actuator located inside the wing.

Indeed, one of our aims was to connect a large number of internal vanes to only a few (in this case only one) rotating valves. This constraint led to a variety of tubing lengths between the oscillating valve and internal actuators, which produced a number of different resonant frequencies in the system. In addition, all the vanes have a small cut, which tends to dampen oscillations. Because the main purpose was to maximize the amplitude of the velocity fluctuation at the slot exit over a wide range of forcing frequencies, it was often desirable to operate the actuator at resonant conditions. It is difficult to predict the fluctuations in velocity amplitude that may occur at the exit of an actuator for a given input pressure and oscillating valve frequency and with a specific system configuration. The system just described can be modeled using the electroacoustic analogy approach as proposed by Kim and Williams [5] and McCormick [14], in which a mechanical system is substituted by an equivalent electrical circuit (see Fig. 10), and the overall transfer function is studied to evaluate the influence of each component on exit velocity. In this analogy, the motion of the fluid is equivalent to the electrical current, and the difference in pressure across the mechanical elements is described electrically by the voltage across the corresponding part of the electric circuit.

In brief (the complete analysis is omitted for brevity), the resonance frequencies of the transmission line depend greatly on the length of the tubing, whereas the geometry of the actuator (slot exit, chamber volume, and plate thickness) strongly affects the peak but not the resonant frequencies.

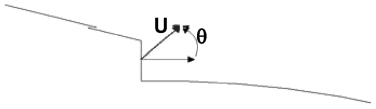

Fig. 8 Definition of the injection angle.

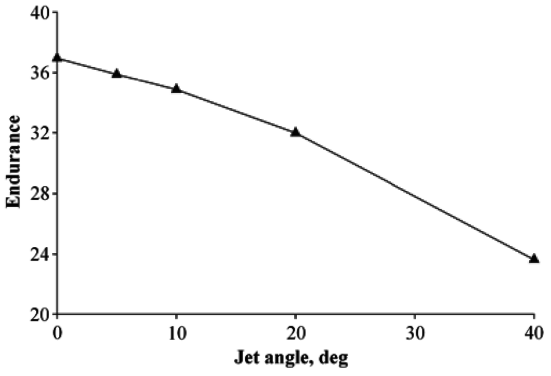

Fig. 9 Jet angle effects, endurance output.

IV. Experiments: Model Design and Tests

The wind tunnel at the Department of Aerospace Engineering, University of Naples Federico II, is a closed-circuit wind tunnel with a closed test chamber. The test section is 1.4 m high and 2 m wide. The turbulence level is about 0.1%. The maximum velocity is 45 m/s.

A. Data Acquisition System

In this section, a rapid survey of the instrumentation used at DIAS is presented. Some of this instrumentation has been used for experiments on steady suction, whereas some only for unsteady-blowing experiments.

For pressure acquisition, a pressure data scanning model ZOC33 thermal control unit by Scanivalve Corporation was used. This is an electronic pressure scanner with a 64-channel sensor.

A multimanometer with 100 sensors and an automatic reading system (accuracy ±1.5 Pa) was also used to capture wake pressures for the measurement and evaluation of drag. For the measurement of the velocity at the slot exit (only for blowing case in this case), a single component hot wire anemometer distributed by Dantec Dynamics was used, calibrated in the range of 0 to 40 m/s in the wind tunnel.

A Spartan device distributed by Instrumentation Devices with 12 channels at 16 bits and a sampling rate of up to 10 kHz was used for data acquisition and processing.

B. Rotating Valve Design

Figure 11 shows how the rotating valve was designed (11a) and built (11b). It has 12 output holes with an internal diameter of 10 mm distributed on 3 rings and 4 input holes with an internal diameter of 14 mm. The valve was designed to guarantee a continuous flow rate and should rotate at about 1500 rpm corresponding to a frequency of the output velocity fluctuation of 100 Hz.

In the pulsed-blowing system, an intermediate tank between the compressor and rotating valve was added to destroy any eventual fluctuating air component, thus ensuring a steady air supply (0–4 bar). The aims are twofold: firstly, to reduce fluctuations due to the

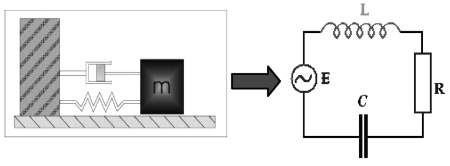

Fig. 10 Electroacoustic analogy [14].

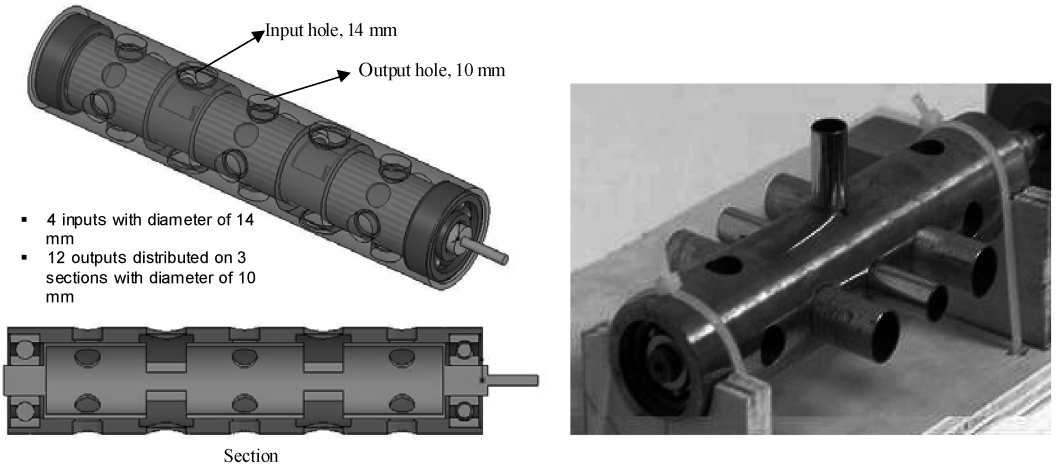

Fig. 11 Rotating valve: a) design, and b) building.

compressed air and, secondly, to measure the pressure directly inside the tank using pressure taps.

C. Model Design and Building

There are many aspects that could be investigated, but some of them would require more than one airfoil construction to carry out these analyses. It was therefore decided to study the influence of only some of the total number of variables (Reynolds number, injected flow frequencies, and momentum) and to postpone studies on the influence of different actuator geometry and position to a later date. The model wing is illustrated in Fig. 12a, and it employs the same airfoil used for the numerical test previously illustrated. The model is 0.60 m in chord and 1.40 m in span and has a maximum thickness of about 20% located at 40% in chord. Onto this baseline profile an interchangeable part with a blowing actuator was designed (see Fig. 12b). This part was designed to be interchangeable to be able to try out different actuator geometries on the same model in the near future. The actuators have three main components: an internal chamber, a closing plate, and a slot. The entire span is divided into 12 internal cylindrical chambers, each one with a 0.115-m span and 13-mm radius (see Fig. 12c). The exit slot is located at approximately 60% of chord, with a cut width of 0.8 mm. The closing plate with the slot cut is about 3.5 mm thick (see Fig. 12c). Each chamber is connected with the rotating valve via an input "tube" with an internal diameter of 10 mm (Fig. 12c) and a 2.0-m-long distribution line (connection tube) that connects the rotating valve to the chambers.

The wing model building process is illustrated in Fig. 13. The assembled model with the connection tube is illustrated in Fig. 13c, in which it is possible to see the plate that separates one internal chamber from the other. In Fig. 13d, the closing plate and slot exit profile are illustrated in more detail.

The model was positioned in the wind tunnel as shown in Fig. 14a and, in Fig. 14b, the special features of the actuation system are illustrated, along with the rotating valve driven by a dc motor and the connection tube between the valve and internal chambers. The model dimensions are 0.60 m in chord and 1.40 m in span, and 54 pressure taps were distributed along the midsection at 0.70 m in span (2-D conditions).

The drag was measured through the wake rake using 89 pressure taps connected to the multimanometer. Preliminary tests were carried out to investigate the exit slot velocity at different valve rotation frequencies (input voltage of the motor that drives the valve). All of the experimental tests were done twice to test the repeatability and reliability of the data, and variations between different runs were negligible. The necessary jump in inlet pressure was obtained using a blower and the valve driven by the standard dc motor in the range 0–12 V, corresponding to a rotation rate of 0–120 Hz . The exit slot

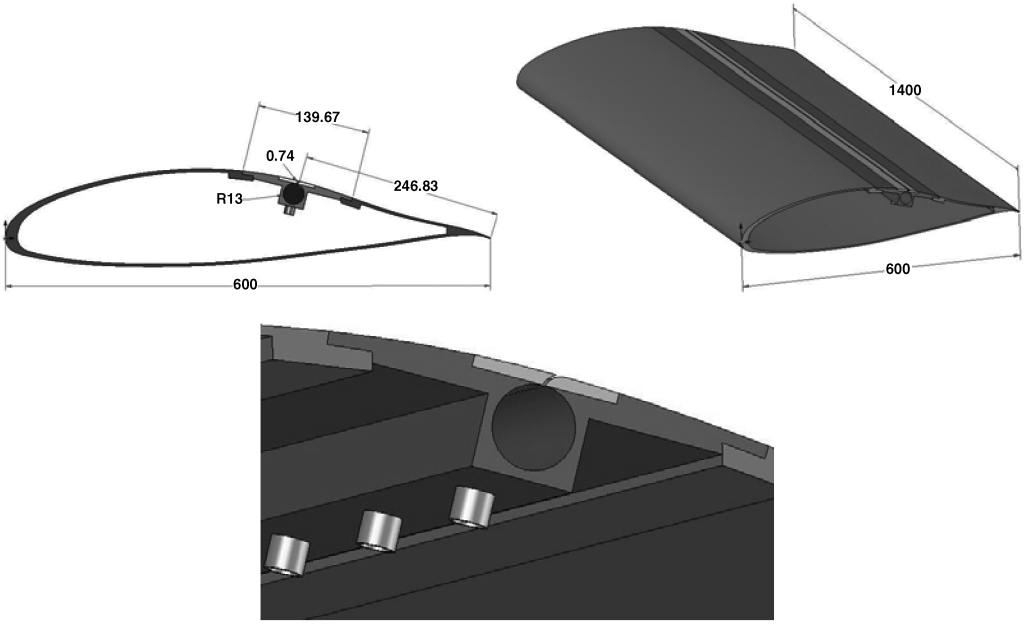

Fig. 12 Design of the model (measurements in mm): a) wing section; b) wing design, global view; and c) wing design, chambers section.

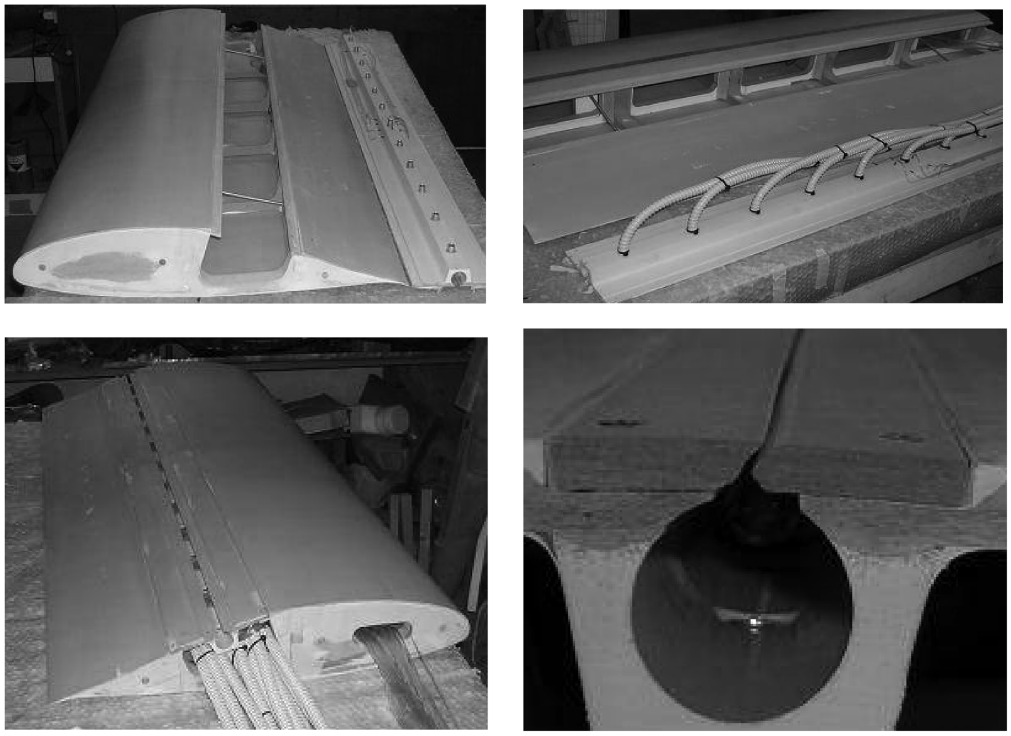

Fig. 13 Building of the model: a) wing building, open model; b) wing building, tubing connection; c) final model; and d) slot.

velocities measured refer to the chamber near the midspan of the airfoil (0.70 m), where the pressure taps for pressure measurement were also located.

An example of the exit slot velocity at 9 V (equal to 120 Hz) is reported in Fig. 15. The range considered for the reduced frequency F^+ is 0–1.5 for which, for the computation of reduced frequency, the reference length is the distance between the exit slot and trailing edge (0.23 m) and the reference for the velocity is freestream velocity ($Re_\infty = 8 \times 10^5$ means $U_\infty = 18.6$ m/s).

D. Experimental Tests: Control Off

In this section, the results for the uncontrolled case are presented. The aerodynamic characteristics presented relate to lift, drag, polar, and endurance curves with and without control. The drag is calculated from data measured in the wake. The lift is obtained from the integral of the pressure measured on the airfoil. Two configurations were tested: the clean configuration with no imposed transition and a stripped configuration with transition imposed at 4% of chord. Figure 16 compares the clean and stripped configurations for lift curve and polar curve with the freestream Reynolds number equal to 8×10^5 for the uncontrolled case. As can be seen, the airfoil is highly dependent on surface roughness and laminar-turbulent conditions. Without imposed transition, the airfoil seems to reach stalling point at $\alpha = 9$ deg but, as illustrated in Fig. 16a, the real stall occurs at near $\alpha = 30$ deg. The phenomenon occurring at α equal to 9 deg is only the sudden changing of the flowfield from being completely attached to a state of separation (trailing-edge separation); beyond this angle, the peak continues to grow until, at $\alpha = 32$ deg, the pressure peak drops.

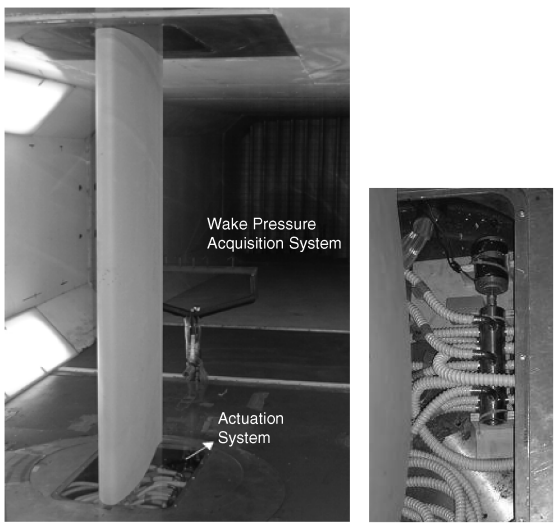

Fig. 14 Setup of the model: a) in the wind tunnel, and b) with a detailed view of the excitation system arrangement.

E. Experimental Tests: Control On

In this section, the results relating to the application of control are presented. Different configurations were tested, with and without imposed transition, both with steady and unsteady blowing at different reduced frequencies and momentum coefficients. Figure 17 shows the lift coefficient (Fig. 17a) and endurance curve (Fig. 17b) for the clean configuration under four conditions: no control applied (baseline), steady blowing with a mean velocity of 18 m/s, an excitation frequency of 50 Hz, and an excitation frequency of 120 Hz. In all cases, the root mean square of the momentum coefficient is approximately 0.2%. The same results are reported for the configuration with imposed transition, in Fig. 18. Lift curves show that the application of unsteady blowing produces greater improvements than steady controls for all configurations,

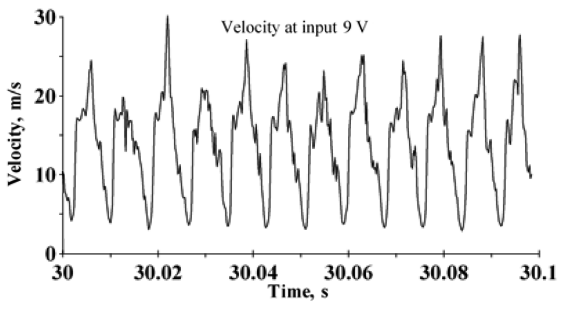

Fig. 15 Exit slot velocity at a frequency of 120 Hz.

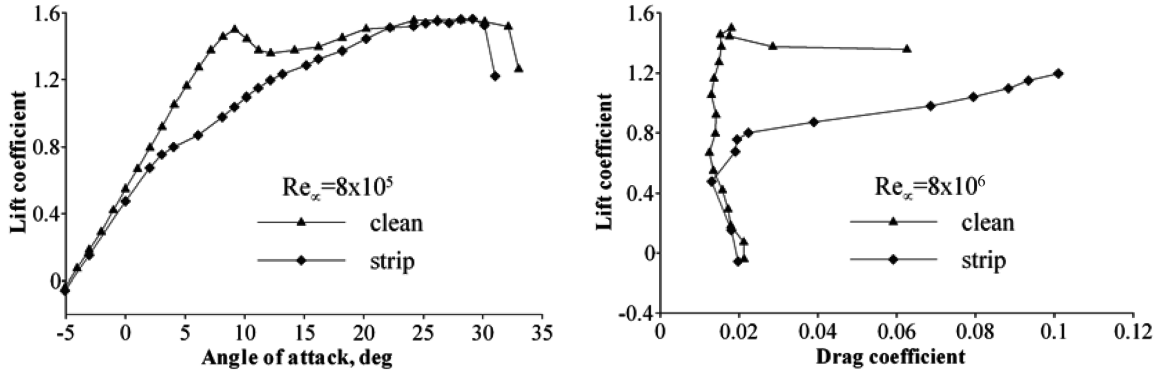

Fig. 16 Experimental tests, control off, comparison of strip-clean curves: a) lift coefficient, and b) polar.

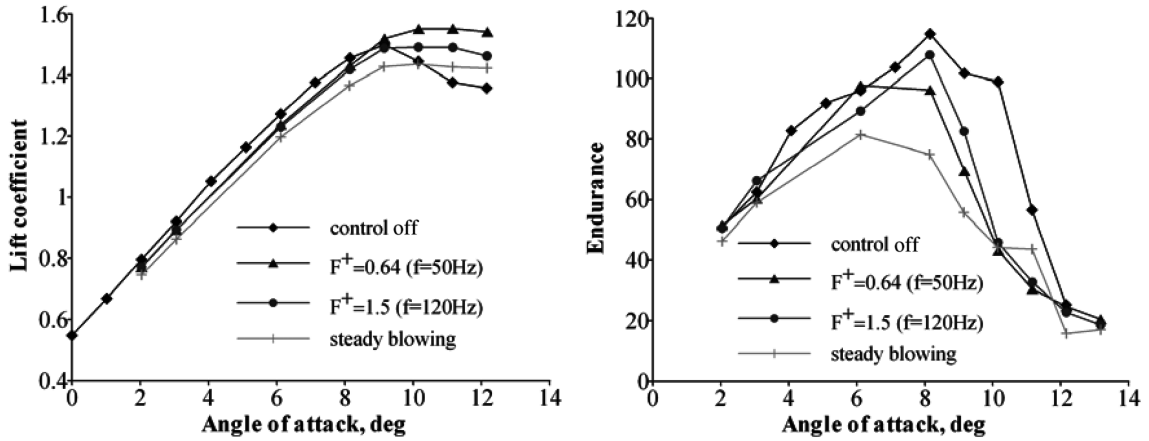

Fig. 17 Experimental tests, control on, curve for the clean configuration: a) lift coefficient and b) endurance.

particularly at a 50 Hz frequency. However, if polar curves are considered alone, this improvement is seen only for the configuration with fixed transition. In fact, when actuation is applied to the clean configuration, this shows enhanced performance in terms of lift, but is worse in terms of endurance (due to increased drag).

In contrast, for the stripped configuration, the application of steady/unsteady blowing produces an improvement in both lift and endurance characteristics. This could be due to the fact that with a clean configuration the laminar bubble extends from the leading edge to near (and maybe including) the slot exit, and this inhibits the application of control, producing a slight positive effect on lift (increasing the pressure peak) but at the same time substantially increasing drag. A possible explanation for this could be that weak blowing inside or near the bubble produces a higher boundary-layer thickness at bubble reattachment after transition, and this produces more drag.

1. Frequency Effect

For the configuration with transition imposed, the effect on aerodynamic performance of varying frequency at certain angles of attack was studied in great depth. The angles of attack chosen

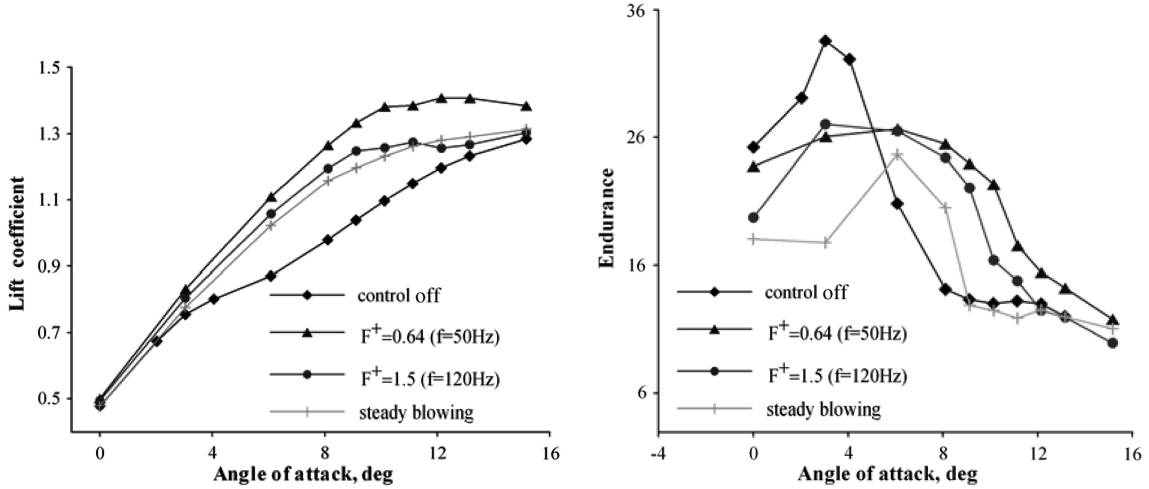

Fig. 18 Experimental tests, control on, curve for the fixed transition configuration: a) lift coefficient, and b) endurance.

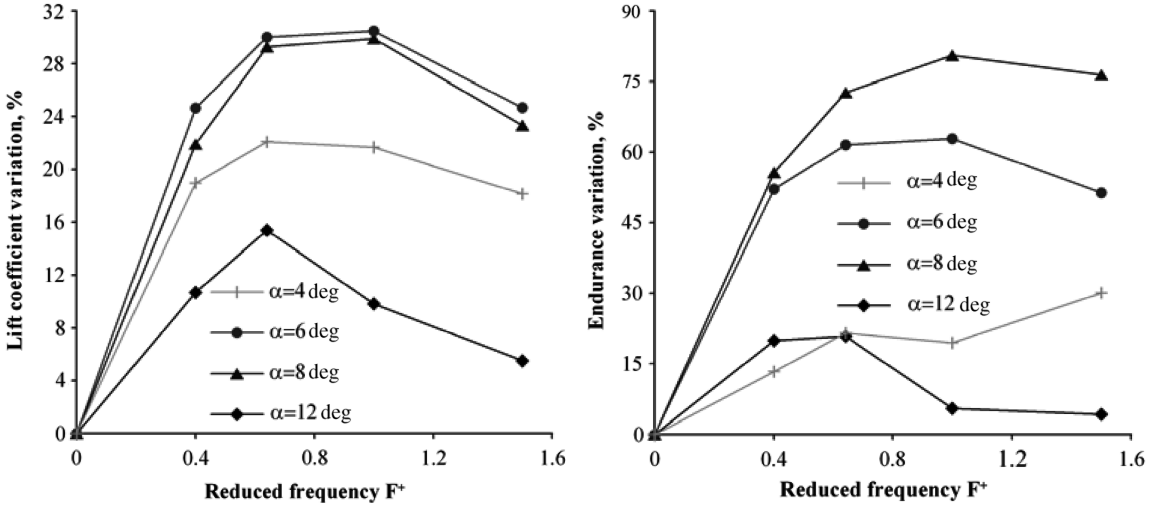

Fig. 19 Percentage variation under the condition of no control applied: a) lift, and b) endurance.

allowed us to analyze the effect under the condition of weak separation (close to trailing edge) corresponding to $\alpha = 4$ deg and under the condition of strong separation (upstream of slot exit) corresponding to $\alpha = 12$ deg. At each angle of attack, different actuation frequencies were tested in the range of 0–120 Hz (0–1.5 in terms of reduced frequency F^+), starting from the case with the valve closed (0 Hz, no control applied). The results are presented in Figs. 19a and 19b and show a percentage change in lift and endurance compared with the condition of no control applied. It can be seen that the positions of greatest improvement change as angles of attack vary, moving from 30 Hz (for the curve relating to $\alpha = 12$ deg) to 120 Hz (for the curve relating to $\alpha = 4$ deg), whereas for the curves relating to $\alpha = 6$ and 8 deg, the maximum stays at 80 Hz. This is due to the fact that higher angles of attack produce a more extended separated area and, because the main shedding frequency of the separated flow also depends on the distance between the separation point and trailing edge, the optimal actuation frequency changes with the angle of attack. In particular, the higher the angle of attack and the separated area, the lower the optimal actuation frequency is. Another interesting result is that, even if the improvement in endurance is also appreciable for $\alpha = 4$ and 12 deg, the effect is stronger when the angle of attack is 6 or 8 deg for which the improvement is more than 60%. This is due to the fact that the exit slot position is fixed, and when the angle of attack is 4 deg the separation point is near the trailing edge, far downstream from the exit slot. Instead, in the case of $\alpha = 12$ deg, the separation point occurs upstream of the slot exit, whereas for angles of attack of 6 and 8 deg the separation point is close to the exit slot location. This suggests that the exit slot position is also extremely important in controlling the flow and that, in principle, a movable exit slot position would be desirable to obtain an optimal control system under all flight conditions.

2. *Reynolds Number Effect*

The effect of the freestream Reynolds number was considered and the results are reported in Fig. 20. The angle of attack was fixed at $\alpha = 8$ deg as was the exit slot mean velocity. The maximum lift increment obtainable for the actuation frequency range of 0–120 Hz was reported under these conditions for four different freestream Reynolds numbers (from 8×10^5 to 12×10^5). The values in Table 2 and Fig. 20 summarize the results obtained. It can be seen that, when the freestream Reynolds number increases, the maximum lift coefficient increment ($\Delta Cl_{\max}$ in Table 2) decreases.

The most significant jump in the lift coefficient increment is when the ratio between the injection velocity and freestream velocity rises from 0.45 to 0.53. In fact, increasing this ratio by 17% produces a 100% increase in lift coefficient, whereas when

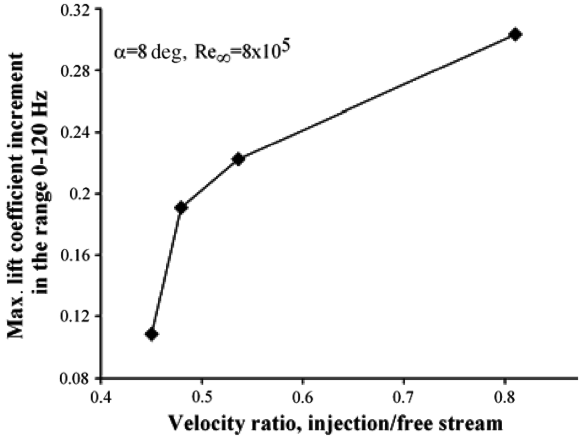

Fig. 20 Reynolds number effect, maximum lift increment obtainable for the actuation frequency range of 0–120 Hz.

the velocity ratio goes up from 0.53 to 0.81 (an increase of 52%) the lift increment increases by only about 36%. Higher velocity means not only greater improvement, but also higher power input. Thus, as far as this analysis and this case are concerned, a velocity ratio close to 0.5–0.6 emerges as a good compromise in terms of cost/benefits.

F. Comparison with Numerical Results

In this section, the comparison of the experimental results with the numerical simulations both for the controlled and uncontrolled cases (with strip on) is presented in Figs. 21 and 22. In all figures the continuous line relates to the numerical simulation and the marked line to the experimental results.

In Fig. 21, the results refer to the case with the control off. In Fig. 21a, the lift curves are reported. In Fig. 21b, the curves of endurance are presented over the range 0 to 15 deg. Although the numerical simulations were also performed for higher angles of attack, the drag can only be measured accurately up to 15 deg (at

Table 2 Reynolds number effect

	U_{mean}, m/s	U/U_∞	U_∞, m/s	$f_{\max}$, Hz	$\Delta Cl_{\max}$
A	15	0.81	18.5	80	0.30
B	15	0.53	28.3	120	0.22
C	15	0.48	31.2	120	0.19
D	15	0.45	33.3	80	0.11

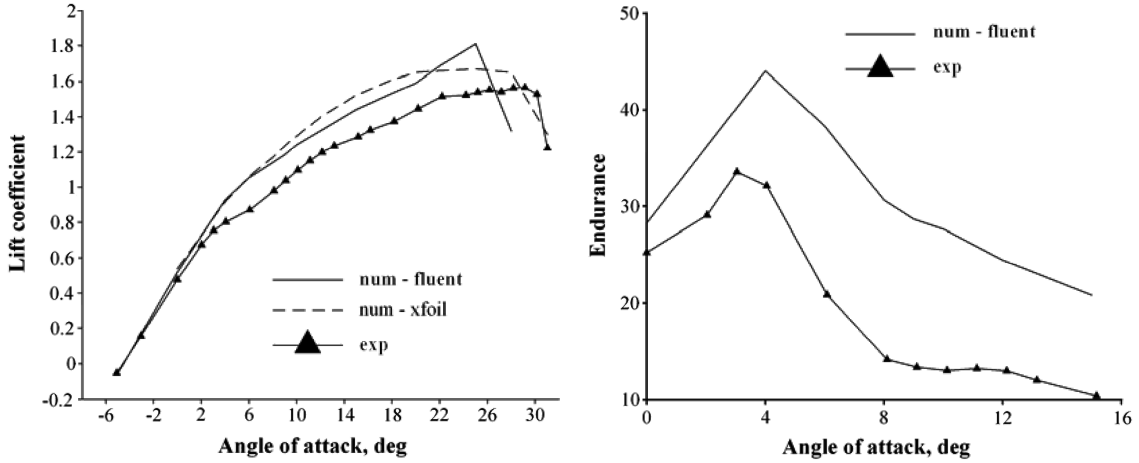

Fig. 21 Control off and strip on, comparison of experimental results with the numerical simulations: a) lift coefficient, and b) endurance.

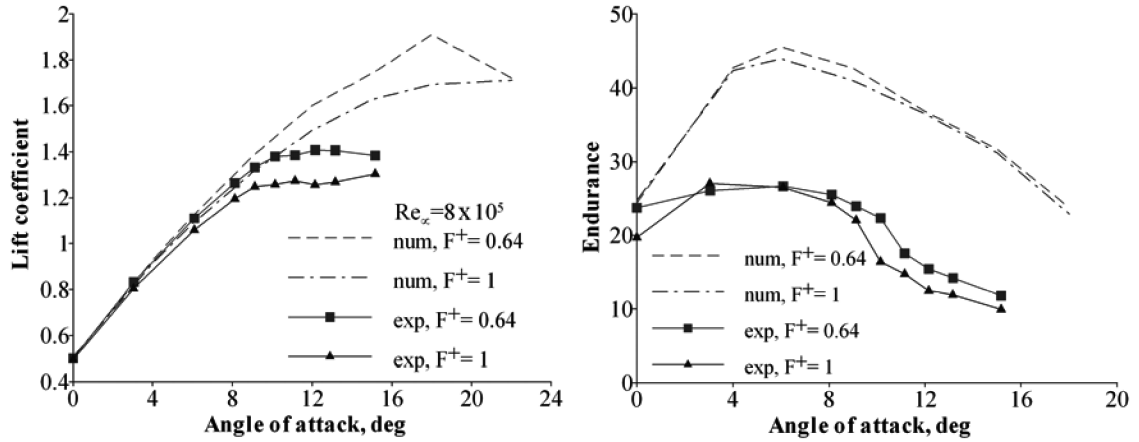

Fig. 22 Control on and strip on, comparison of experimental results with the numerical simulations: a) lift coefficient, and b) endurance.

higher angles the wake becomes too large to be captured correctly). The figures for this configuration are consistent overall with the experimental data; the good lift performance and the gradient of the lift curve are captured well by the numerical simulation. Some problems emerge when the drag prediction is also taken into consideration; in fact, Fig. 21b shows how the endurance is overestimated by the numerical simulation compared with the experimental tests, even though the general pattern is captured well. These differences are mainly due to the turbulence model, airfoil shape, and model building. It is important to point out that, although numerical simulation is intrinsically characterized by errors due to the use of the turbulence model developed for boundary layers and also used for massive separation (small errors in the prediction of velocity fields may lead to detectable errors in drag prediction), it is also true that the tested airfoil is highly sensitive to the experimental conditions, and even barely detectable differences between the theoretical shape and "built" shape (actuator section, surface roughness, and airfoil curvature) may influence the results.

In Fig. 22, the comparison of the results with the control activated are reported. In Fig. 22a, the lift curves are reported with the control activated at a frequency of 50 and 120 Hz together with the baseline (control off). The figure shows, as the numerical simulation predicts, that the control is more effective than the experimental evidence shows.

For both excitations (continuous lines), lift enhancement is positive even close to the stall angle, whereas in the experimental tests the control is effective up to an angle of attack of 15 deg. The same behavior is shown in Fig. 22b, in which the numerical simulation overestimates the gain in endurance when the control is applied. In spite of this discrepancy, the general pattern of behavior is captured well; in fact, all of the lift coefficient curves and endurance curves suggest that the solution using 50 Hz is more effective than the one at 120 Hz and also the ineffectiveness of control at low angles of attack is captured by the numerical simulation. Overall, the numerical calculations have fulfilled their main purpose, that is, to predict the qualitative behavior of the system to establish the most suitable configurations for testing in the wind tunnel. What remains are the quantitative discrepancies with experimental results.

An important point to note is that in the numerical law of control a sinusoidal wave without distortions was considered, whereas the wave form is slightly different under real flow conditions. Future improvements could include an inlet injection that matches precisely the experimental injection jet measured in the wind tunnel (at the slot exit). Some other improvements that could be adopted would be to use some more sophisticated techniques that are currently very popular in this field of research, such as large eddy simulation or the less expensive (in the sense of computational cost) detached eddy simulation. These will be the subject of future studies.

V. Conclusions

A numerical and wind-tunnel experimental investigation was performed for unsteady blowing. Unsteady blowing was investigated theoretically by modeling the behavior of the whole system numerically using RANS computations and experimentally by wind-tunnel tests on a 2-D wing. Unsteady blowing was obtained using a rotating valve, and the theoretical performance of the whole unsteady-blowing system was examined using the electroacoustic analogy to model the system from the oscillating valve to the actuator outlet. A combination of a lumped-element model for the actuator and a distributed model for the tubing was used to obtain a transfer function for the overall pulsed-blowing system. This allowed the analysis of the functional dependence of the whole system on geometrical parameters (tubing length, cavity volume, and slot exit)

and showed that the ratio between the injection slot velocity and input pressure could be maximized once the system operates in the proximity of resonant conditions. The tubing length seems to produce the most significant effect on resonant frequencies, whereas the slot exit and cavity volume mainly affect the resonant peak amplitude. Theoretical considerations suggest that the effectiveness of pulsed blowing depends mainly on the extent of the separated area, freestream Reynolds number, excitation frequency, and strength of injected flow. All this can be summarized via two dimensionless parameters: reduced frequency and momentum coefficient. Numerical and experimental tests were performed to illustrate the behavior of the system when these two parameters are varied by changing the compressed air pressure, valve frequency rotation, and angle of attack. What emerges is that the best actuation frequency varies depending on the type of aerodynamic performance to be optimized (efficiency, lift, or endurance). During this study, many interesting new aspects were highlighted by the experimental results. Nevertheless, there are still others that have not yet been investigated due to the highly complex nature of the problems. The influence of slot cut shape and its position or the influence of chamber volume and tubing length, for example, are some of these, and they will be investigated in the near future. Unsteady blowing via a distributed system is an effective tool to delay separation, with the advantage of being built mainly of mechanical parts (with only a rotating valve to be electrically powered), and requires pressurized air that could be directly obtained through a fan in a real flying wing or picked up by the propulsion system. The main limitation of this system is the presence of tubing because, for practical implementation on a real flying wing, the large number of tubes reduces the available space inside the wing. At the same time, the system with connection tubes is more effective when it works in resonant conditions, which are highly sensitive to the system parameters. For real applications, it would be more suitable to have a system in which both the mechanical complexity and weight of the entire system are reduced. Following these considerations, a new device is being designed, and it will soon be built and tested.

Acknowledgment

This work has been partially sponsored by CIRA.

References

[1] Eppler, R., "Airfoils with Boundary Layer Suction, Design and Off-Design Cases," *Aerospace Science and Technology*, Vol. 3, No. 7, Oct. 1999, pp. 403–415. doi:10.1016/S1270-9638(99)00105-4

[2] Seifert, A., and Wygnanski, I., "On Delay of Airfoil Stall by Periodic Excitation," *Journal of Aircraft*, Vol. 33, No. 4, 1996, p. 691.

[3] Seifert, A., Bachar, T., Koss, D., Shepshelovich, M., and Wygnanski, I., "Oscillatory Blowing: A Tool to Delay Boundary-Layer Separation," *AIAA Journal*, Vol. 31, No. 11, 1993, pp. 2052–2060.

[4] Tinapp, F., and Nitsche, W., "Separation Control on High Lift Configuration by Periodic Excitation," *12DGLR-Fach-Symposium der AG STAB*, Notes on Numerical Fluid Mechanics, Vol. 77, Springer–Verlag, Berlin, Nov. 2000, pp. 42–49.

[5] Kim, B. H., and Williams, D. R., "Large Amplitude Pneumatic Oscillator for Pulsed-Blowing Actuators," AIAA Paper 2002-2704, 2002.

[6] Gad-el-Hak, M., Pollard, A., and Bonnet, J. P. (eds.),*Flow Control: Fundamentals and Practices*, Lecture Notes in Physics, Vol. m53, Springer–Verlag, Berlin, 1998.

[7] Wu, J. Z., Lu, X. Y., Denny, A. G., Fan, M., and Wu, J. M., "Post-Stall Flow Control on an Airfoil by Local Unsteady Forcing," *Journal of Fluid Mechanics*, Vol. 371, 1998, pp. 21–58. doi:10.1017/S0022112098002055

[8] Wu, J. Z., Vakili, A. D., and Wu, J. M., "Review of the Physics of Enhancing Vortex Lift by Unsteady Excitation," *Progress in Aerospace Sciences*, Vol. 28, No. 2, 1991, pp. 73–131. doi:10.1016/0376-0421(91)90001-K

[9] Miranda, S., *Active Control of Separated Flow over a Circular-Arc Airfoil*, Master's Thesis, Virginia Polytechnic Institute, Blacksburg, VA, 2000.

[10] Schatz, M., and Thiele, F., "Numerical Study of High Lift Flow with Separation Control by Periodic Excitation," AIAA Paper 2001-296, Jan. 2001.

[11] Ekaterinaris, J. A., "Prediction of Active Flow Control Performance on Airfoils and Wings," *Aerospace Science and Technology*, Vol. 8, No. 5, July 2004, pp. 401–410. doi:10.1016/j.ast.2004.02.003

[12] Liu, Y., and Sankar, L. N., "Computational Evaluation of the Steady and Pulsed Jet Effects on the Performance of a Circulation Control Wing Section," Georgia Institute of Technology, Paper 27, 2005.

[13] Menter, F. R., "Two-Equation Eddy-Viscosity Turbulence Models for Engineering Applications," *AIAA Journal*, Vol. 32, No. 8, 1994, pp. 1598–1605.

[14] McCormick, D. C., "Boundary Layer Separation Control with Directed Synthetic Jets," AIAA Paper 2000-0519, Jan. 2000.